JOURNAL OF MATERIALS SCIENCE **35** (2000) 3963–3975

Morphology and texture of nanocrystalline copper prepared electrochemically from oxides

W. GÜNTHER*, N. PFÄNDER, G. WEINBERG
Fritz-Haber-Institut der Max-Planck-Gesellschaft, Faradayweg 4-6, D-14195 Berlin, Germany
E-mail: Wulf.Guenther@vacuumschmelze.com

R. LIEDTKE, J. NISSEN
Technische Universität Berlin, Zentraleinrichtung Elektronenmikroskopie, Strasse des 17. Juni 135, D-10623 Berlin, Germany

R. SCHLÖGL
Fritz-Haber-Institut der Max-Planck-Gesellschaft, Faradayweg 4-6, D-14195 Berlin, Germany

The electrochemical reduction of metal oxides provides an appropriate technique for the production of nanocrystalline mesoporous metals at room-temperature. Polycrystalline sintered CuO and Cu_2O single crystals were reduced to Cu in this study. Electron microscopy and diffraction results demonstrate the dependence of the metal microstructure on the preparation and post-treatment conditions. The size and microstrain of the crystallites are controlled mainly by the preparation temperature. This method enables the reproducible production of medium-scale nanocrystalline metals independent on critical process parameters.

1. Introduction

Nanocrystalline metals have attracted the interest of both chemists and physicists for years. However, only very few preparation methods have been developed which are capable of producing larger amounts (>1 g/h) of unstabilized nanocrystalline metals with high purity [1, 2]. Electrochemical techniques have been shown to be an useful alternative to inert gas condensation, precipitation, or milling. The main advantage of electrochemical synthesis is its relative simplicity. In addition, it is possible to carry out the preparation under ambient conditions. Pulsed electrodeposition [3] (fluid-solid transition) has been shown to result in a dense nanocrystalline material. Recently a new concept was developed to produce *mesoporous* metals and oxides via *solid-solid* bulk transformations. This may be accomplished by employing electrochemical reduction and reoxidation of transition metal oxides or salts with low formation enthalpies [4, 5].

The morphology of the materials produced with the latter method has been demonstrated indirectly by performing density calculations and a variety of analytical techniques such as line broadening in x-ray diffractograms and BET measurement of the surface area. In addition, it is well known that the reactivity of compounds obtained by this method is significantly higher than those produced by other techniques [4, 5]. No direct observation of the nanocrystals and the mesopores has been made. An accurate knowledge of the crystal size and shape as well as of the pore structure is necessary, however, to determine the viability of using this material for a number of applications. The results of electron microscopy and x-ray diffraction (XRD) analysis of electrochemically produced Cu are presented in this paper. Morphological modifications are discussed in terms of possible reaction mechanisms. Observed changes of the microstructure as a result of the use of different preparation and post-treatment conditions is also discussed. The consequences of these treatments and various morphologies on the oxidation behavior of the Cu samples is also discussed.

This work considers a quantitative, solid-solid bulk reaction. This represents a qualitative difference to the electrochemical surface reactions typically studied. In contrast to the latter, the reaction presented here proceeds far from the solid-electrolyte interface. Reaction is, therefore, diffusion controlled. Surface effects such as dissolution, deposition or reactions with the electrolyte ions play only minor roles.

2. Experimental

Nanocrystalline Cu was prepared by the electrochemical method described in detail in ref. [4]. The reaction was performed in aqueous electrolytes in a three-electrode cell with Pt as counter electrode and Hg/HgO as reference electrode (for $T < 0$°C a Pt foil was used). Pressed and sintered cylindrical pellets of polycrystalline CuO served as working electrodes. The cell was placed in a cryostat in order to vary the temperature

* *Present Address:* Dr. Wulf Günther, Vacuumschmelze GmbH, Postfach 2253, D-63412 Hanau, Germany.

between −40 and 65°C. The cell was purged with N_2 to avoid a reoxidation of the working electrode.

Standard electrochemical reduction was performed in the potentiostatic mode in 0.1 M KOH (for $T < 0$°C 1 M KOH in an ethanol/water mixture) in order to obtain homogeneous products without changes in the potential during the preparation. The pellets were contacted electrically using Pt wires. Two contacts in the middle of the disc (top and bottom) were applied in order to avoid problems arising from the strong dependence of the evolution of the CuO/Cu (insulator/metal) interface and the resulting current flow through the electrochemical cell on the number and local distribution of the electrical contacts. After starting at a rather high potential (vs. Hg/HgO) where no reaction occurs, the potential was decreased slowly until a reduction current was observed. The reaction was immediately stopped and the experiment was started at a working potential 50 mV lower than the potential determined before. This procedure was chosen in order to eliminate the temperature influence on the electrochemical potentials.

The reduction potential and electrolyte used were varied in order to investigate their influence on the product. Galvanostatic runs with current densities of 1–400 mA/g were performed additionally (especially for electron microscopy studies).

Cu_2O single crystals were grown by molten salt synthesis. 0.5 g Cu powder and 10 g KOH were placed in a corundum crucible with a lid (not absolutely tight to allow a limited gas exchange) and heated to 450°C. The melt was cooled after 40 h to ambient temperature, and the solidified KOH was removed with water. The solid product consisted of flat Cu_2O (ca. $1 \times 1 \times 0.1$ mm^3) and CuO crystals. Most crystals were twinned, however; the biggest untwinned crystals had an area of 0.5 mm^2.

X-ray diffractograms were performed at room temperature with a Siemens D 5000 (Cu $K_{\alpha 1}/K_{\alpha 2}$ radiation) with a scintillation detector in reflection mode. LaB_6 was used for instrumental correction. Pellets were investigated in the as-prepared state as well as powdered to check the bulk character of the transformation. The anisotropic crystal size distribution and microstrain were evaluated with a programme [6] based on the Fourier method by Warren and Averbach (shortly described in ref. [3]; see references therein). The anisotropic crystal size and microstrain were determined according Williamson and Hall [7]. For both methods the Bragg reflex pairs 111/222 and 200/400 were analyzed in order to obtain size and strain parameters perpendicular to {111} and {100}, respectively. The influence of stacking and twin faults on the crystal size (actually the column lengths) computed by the Warren-Averbach approach was further corrected by a method of Warren [20] giving an isotropic volume weighted column length and finally the volume weighted grain size $<D>_{\mathrm{Vol}}$. The latter is usually determined by XRD methods. The median of the distribution function D_{Med} was calculated assuming a log normal distribution for the grain size [3]. This value represents an averaged grain size. $<D>_{\mathrm{Vol}}$ was calculated also from the anisotropic size values from the Williamson-Hall calculation.

The products were examined by optical microscopy and scanning electron microscopy (SEM, Hitachi S 2700 and S 4000) at 10–20 kV. Sintered pellets of CuO (10–50 mg) or single crystals of Cu_2O were reduced partially or totally (galvanostatic mode, 50–200 μA, 0.1 M NaOH). In some cases the pellets were broken, and the fresh profiles were studied. Energy-dispersive x-ray analysis (EDX) of the Cu-L and O-K signals was performed using an EDAX DX-4 system with 5 kV acceleration voltage.

Transmission electron microscopy (TEM) and electron diffraction (ED) were performed in a JEOL 200B with 150 kV as well as in a Philips CM 200 LaB_6 with 200 kV acceleration voltage. Sintered CuO pellets with a diameter of 3 mm and a thickness of 0.1–0.3 mm were dimpled and subsequently sputtered with a 5 keV Ar^+ ion beam at 30 μA gun current under an incident sputtering angle ranging from 4 to 2°. These samples were partially electrochemically reduced (galvanostatic mode, 100 μA, 0.1 M NaOH) to a degree in order that the sharp reaction front [4] be located in the transmissible region, i.e. both CuO and Cu regions could be observed. Subsequently the samples were rinsed in water and acetone, dried, and transferred into the microscope. The total exposure time to air was about 10 min. In another experiment a Cu_2O single crystal was partially reduced, the procedure was the same as described.

To study the oxidation behavior of the copper products a solid electrolyte coulometry system Oxylyt (SensoTech) was used. A carrier gase (Ar, 1 bar) was loaded with 1 mbar O_2. The oxygen consumtion during heating (50 K/h) of the sample was titrated.

In this paper, the term "grain" denotes a crystallite (in the order of magnitude of 1–10 μm) of a polycrystalline sample (CuO) before reaction as well as the same unit after reduction. In contrast to this, the term "nanocrystal" or "particle" referrs to a crystallite of the reduced copper (5–50 nm).

3. Results

3.1. Electrochemistry

The oxide working electrode (cathode) began to convert to copper metal immediately after starting the electrochemical process. Reaction occured with a sharp reaction front starting from the electrical contact. No gas evolution was observed at the working electrode or the platinum leads under normal reduction currents. The reaction was accompanied by gas evolution at the anode. The electrode reactions in the electrochemical cell are formulated as follows (for CuO):

$$\text{Anode:} \quad H_2O \rightarrow 2H^+ + \tfrac{1}{2}O_2 \uparrow + 2e^- \qquad (1)$$

$$\text{Cathode:} \quad 2H^+ + 2e^- + CuO \rightarrow Cu + H_2O \qquad (2)$$

It is remarkable that the color of the educts changed immediatly after applying the current. This occurred parallel to the appearance of the first visible copper traces. Cu_2O (red) turned to dark-red (almost black) and CuO (black with a slight metallic lustre when sintered) became matt black. No correlation with these color changes could be resolved in the current-time or

potential-time curves. This initial period of the electrochemical reaction is dominated, however, by strong overpotential or low currents [4]. This is due to the small area of the reaction front. The effect described is therefore not expected to be visible in the curves.

The presence of an overpotential prevents the exclusion of the electrochemical formation of CuH. This is possible once copper nuclei are formed and enables also the chemical reduction of copper oxide by CuH in a continuous process. There was no evidence for the formation of CuH, however. Only the reactions according to Equation 2 are therefore considered (for a further discussion of mechanism see below).

The mechanical integrity, size and shape of the CuO pellets was retained after reduction (pseudomorphism). The total conversion to Cu was proved by monitoring charge transfer (2 e^-/f.u.) and performing XRD analysis of the products [4]. The pellets had the typical color of copper. A spontaneous surface oxidation occured a few minutes after switching off the current. This results in a darkening of the pellets. Samples prepared at low temperatures ($< -20^\circ$C) turned to black within a few seconds at room temperature. This is a clear indicator of the increased reactivity of these samples.

3.2. Grain Morphology

Both changes of the initial oxide grains or single crystals after reduction and the internal structure of the grains themselves, i.e. the morphology of the nanocrystallites have been studied by SEM.

Reduced polycrystalline CuO pellets are considered first. Fig. 1 shows the surface of a partially reduced pellet. The CuO and Cu parts are clearly discriminated in the backscatter-electron (BSE) image. The reaction front appears sharp when crossing a grain. A gap between both zones is visible both in the secondary electron (SE) and the BSE image (further details of the gap see below). The grains are well separated each from another at the reduced side. This is a sign that the grain volume decreases significantly during the reaction and results in eventual destruction of the grain boundaries. This shrinking also was observed in the bulk by SEM inspection of a fracture edge. It turned out that the relative volume change depends on the current density. High currents result in large shrinkage. Small currents cause less shrinking. Especially large grains show cracks and tears (Figs 1 and 2). The evaluation of SEM images shows a total decrease of the grain volume between 15 and 30% for reduction currents of 1–400 mA/g, respectively.

The surfaces of the grains themselves show a well pronounced substructure at higher magnifications. The CuO grain surfaces are flat and show terraces. The reduced ones assume a lamellar morphology (Figs 2 and 3). This morphology was already described in the previous investigation [4]. Samples prepared at room temperature exhibit a lamella thickness of about 30–100 nm. The lamellas also have a substructure. They appear to represent quasi-two-dimensional arrangements of relatively densely packed nanoparticles.

The contrast of the lamellas is enhanced after storage in air (Figs 2 and 3) or in the electrolyte. This has been attributed to surface oxidation which produces oxide sheets at the external and (porous) internal grain boundaries. Slightly oxidized samples are more useful for studying morphological features by SEM as the surface morphology is not affected by the oxide skin (compare Fig. 2b and 2c). The imaging of the same region after storage in air is limited, however, due to the smoothing of structures as a result of carbon contaminations at irradiated areas (compare Fig. 2b and 2c). Therefore different regions (for example Fig. 2d) were investigated for the time evolution. After extended storage new features (secondary crystals, precipitates) become visible. This results from oxidation and as a result of reactions with H_2O or CO_2.

A detailed study of the reaction front (oxide/metal interface) was performed with partially reduced Cu_2O single crystals. The front was characterized by a gap located at or parallel to the Cu_2O/Cu interface (Fig. 4). The expected changes in relative signal intensities observed by performing an EDX line scan (Fig. 4e) identifies the reaction interface. The interface is not identical with the gap but the latter is situated at the Cu site for the example shown in Fig. 4. The line scan indicates a higher density of Cu in a narrow zone behind the Cu_2O/Cu interface.

Both edges of the "gap" appear to match each one another. This feature it is, therefore a crack and not a solid/fluid/solid or solid/gas/solid interface formed in the course of the reaction. In the latter case the gap was a "moving crack". This represents a case where the reaction most likely terminates as a result of the loss of electrical contact. The sample should easily fall apart.

The morphology of the Cu side is characterized by a rather dense microstructure located between the interface and the crack and the already described lamellar structure behind the crack. The lamellas usually appear parallel to the reaction front. Their intensity and their angles with the surface vary. Their appearance is likely dependent on the orientation of the lamellas in the crystal lattice and relative to the surface (cf. Fig. 3).

3.3. Nanocrystal morphology

Several CuO pellets were partially reduced and subsequently examined by TEM. Unreacted polycrystalline CuO and regions of nanocrystalline Cu were identified by ED (see below). No intermediates (Cu nuclei, Cu_2O or suboxides) were detected.

The nanocrystals were clearly resolved in the bright field images (Fig. 5). An additional impression of the shape and size is provided in the dark field images (Fig. 6). The crystallites appear compact and without regular shape. Several crystallites show interference contrast (Moiré fringes) (Fig. 5b) indicating good crystallinity and a rather flat crystal shape. The diameter distribution of nanocrystals prepared at room temperature is rather broad and lies between 6 and 25 nm.

No regular arrangement of nanoparticles or a regular pore structure was detected. The shape and the arrangement of the crystals show a considerable amount of intergranular space. It is possible that the packing of

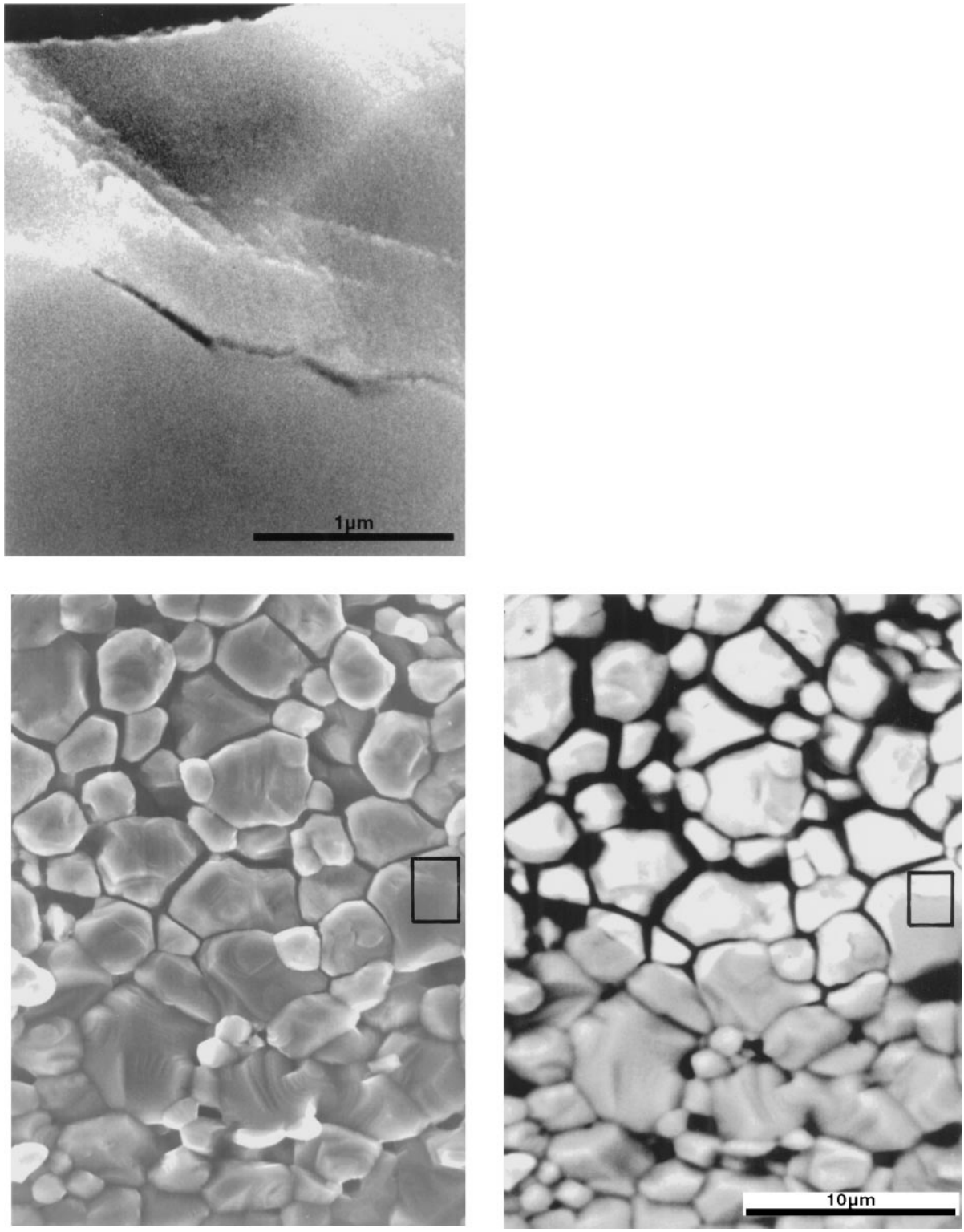

Figure 1 SEM images (bottom left: SE, secondary electron image, bottom right: BSE, backscatter electron image) of a surface of a polycrystalline sintered CuO pellet partially reduced to Cu. Lower part (dark in BSE): CuO, upper part (bright in BSE): Cu. Note the separation of the grains at the Cu site and the tears at the reaction front (top: magnified SE image) due to shrinking.

crystals is much closer in the bulk of a grain than at the edge investigated here with TEM.

3.4. Nanocrystal texture

The ED patterns of nanocrystalline regions (Fig. 5a) are characterized by a series of diffraction rings. The predominant rings are assigned to Cu. Weak rings of re-oxidized Cu_2O (see above) were also identified. Fig. 5 shows an image and the corresponding ED pattern of a region which was formed from a single CuO grain. The non-uniform intensity distribution over the diffraction rings of the nanocrystalline product indicates a rather close orientation distribution around a preferred orientation, i.e. a strong texturing. This has already been proposed based on powder XRD data [4]. The diffraction pattern in Fig. 7 (processed pattern of Fig. 5a) represents nearly the $[01\bar{1}]$ zone ([100]/[011] plane) of the

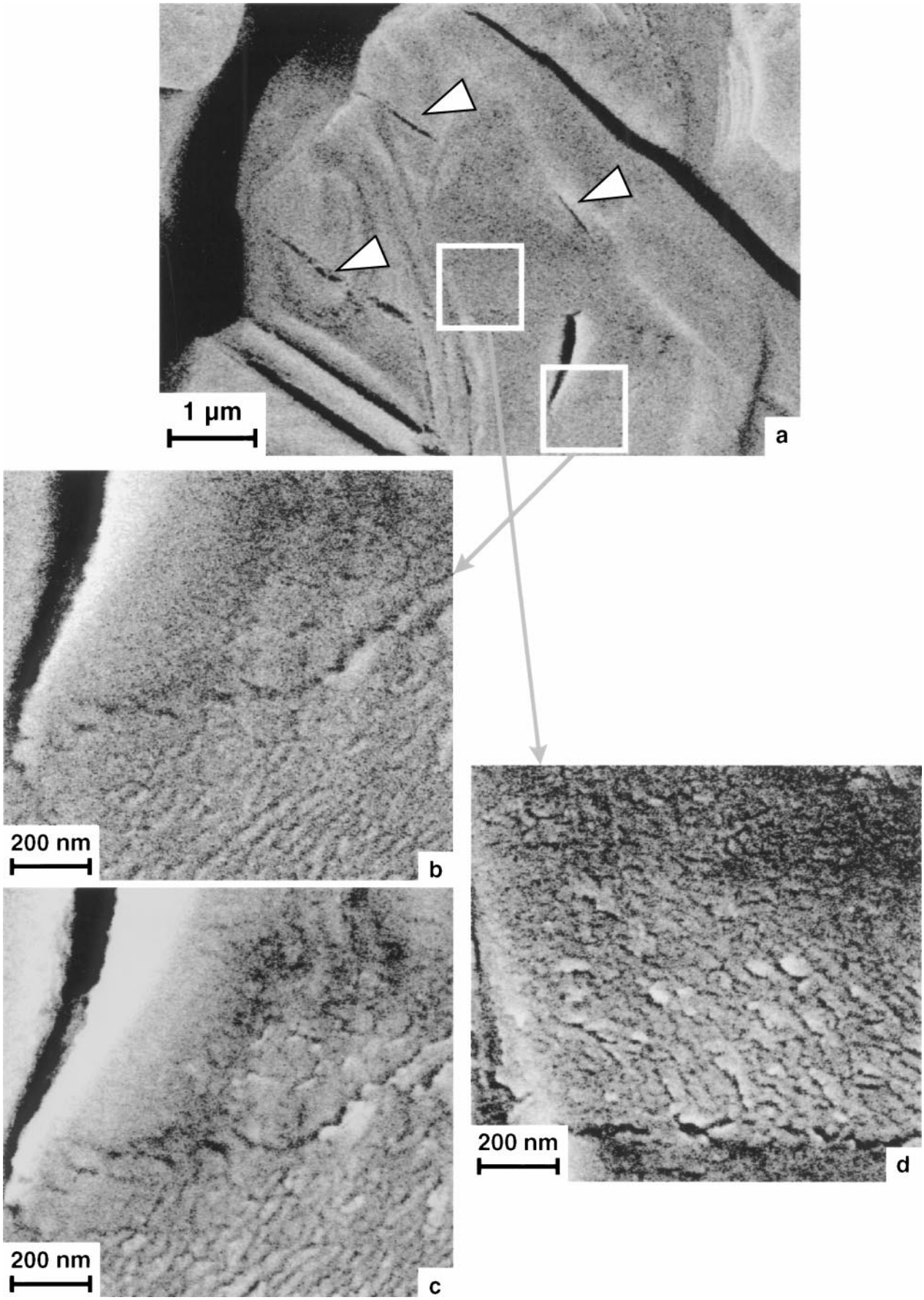

Figure 2 (a) SEM image (SE) of a typical grain of a polycrystalline CuO sample (10-mg pellet) after reduction (galvanostatic mode, 100 μA, air contact 10 min) to Cu. Tears are marked with arrows. (b) Section of a. (c) Same section after 8 days in air. (d) Another section after 12 days in air.

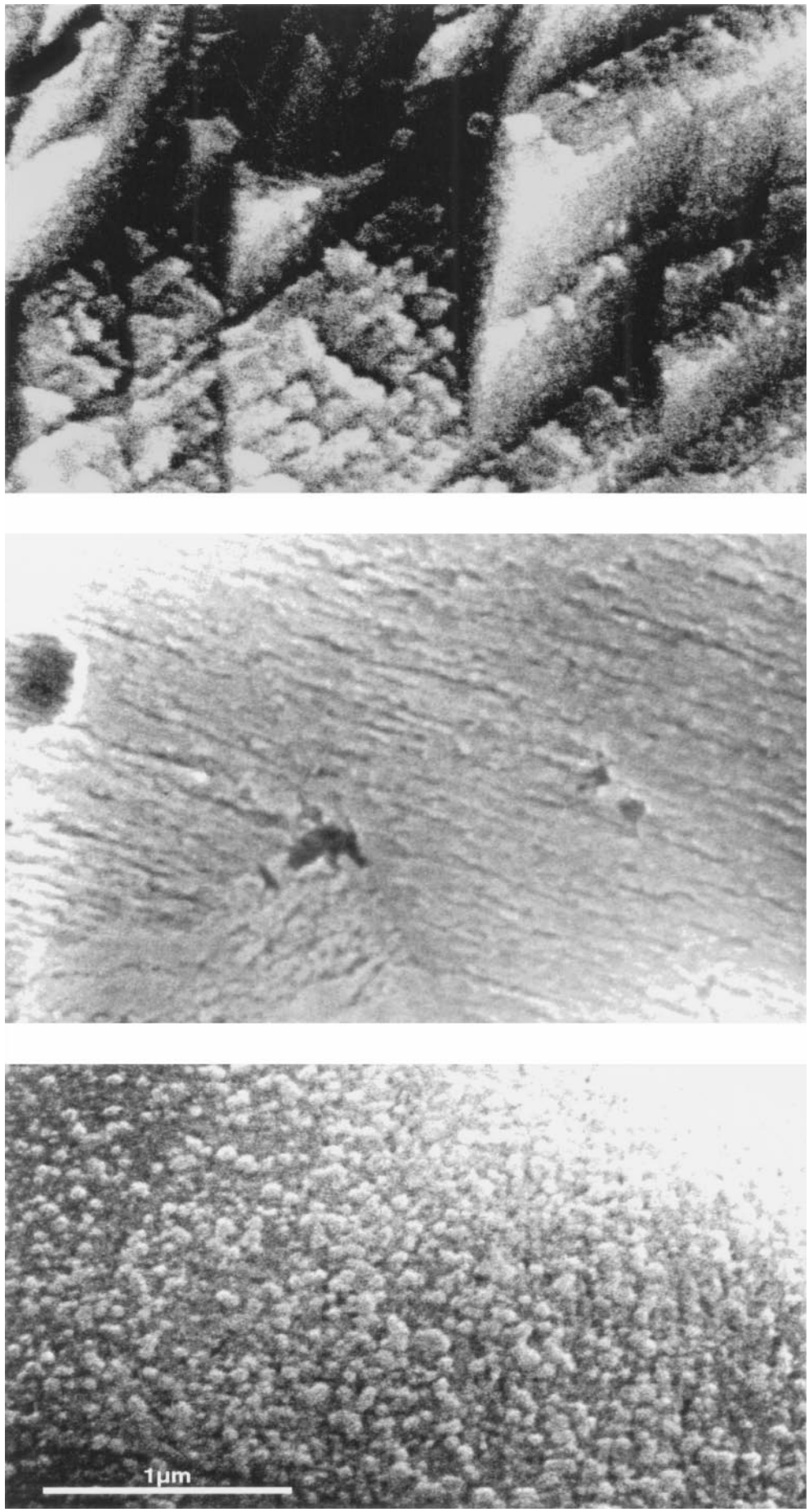

Figure 3 SEM images (SE) of typical surface structures of CuO grains after reduction and storage in air for two weeks. The sphere-like crystallites visible in the bottom image may be already secondary crystals from the reaction of Cu with air.

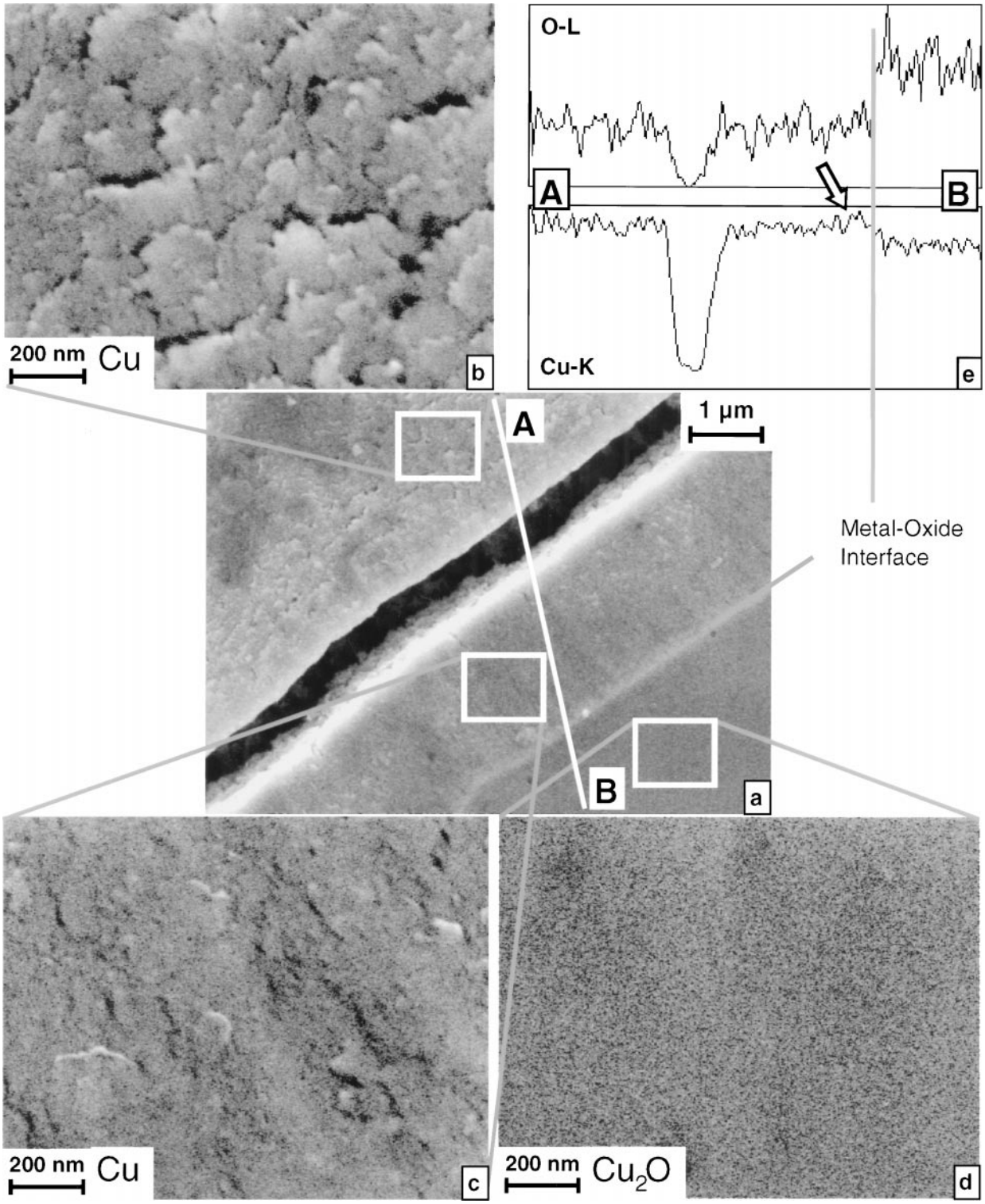

Figure 4 (a) SEM image (SE) of the reaction front on a Cu_2O single crystal (galvanostatic mode, 50 μA, air contact 2 hours). (b)–(d) Sections of (a). (e) EDX line scan over the reaction front. The arrow marks the increased Cu signal behind the oxide-metal interface.

Cu main orientation with a slight canting δ, i.e. the $(\delta_1\, 1\, \overline{1+\delta_2})$ (with δ_1, $\delta_2 \ll 1$) projection. The "spots" which are not visible in a $[01\bar{1}]$ ED pattern of a ideal single crystal are marked with $\oplus$ or $\ominus$. The inability to image these spots arises from the fact that they are located above or below the diffraction plane in the reciprocal space. The other "spots" form the rectangular $[01\bar{1}]$ pattern of a cubic crystal (grid in Fig. 7). This accounts for the systematic absences of the face centered lattice. The orientation distribution function was not analyzed. A Gauss-like distribution with a half width of about 20° may be estimated from the length of the ring segments. The weak inner ring arising from reoxidized Cu, i.e. the 111 ring of Cu_2O (marked in Fig. 7), shows the same intensity distribution as the 111 ring of Cu.

The disadvantage of the described TEM investigation using polycrystalline material as starting compound for the electrochemical reduction is obvious. The nanocrystalline product contains regions arising from different educt grains showing different orientations. Hence a correlation between the preferred orientation of the product nanocrystals and the orientation

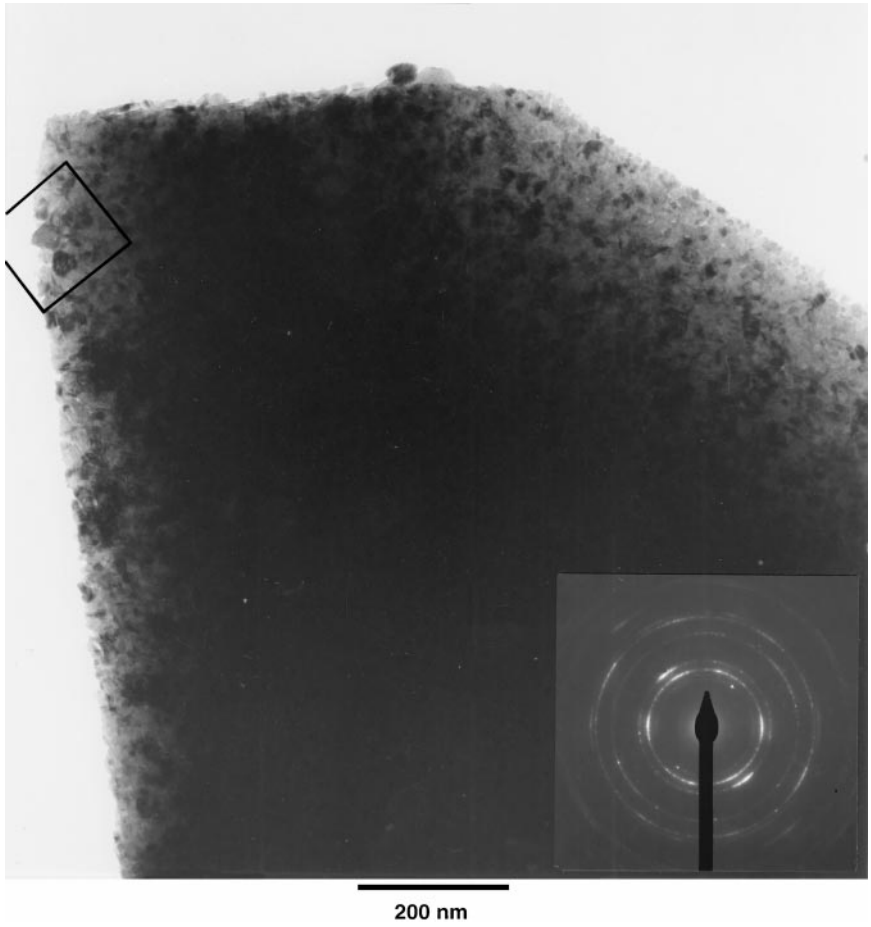

(a)

(b)

Figure 5 (a) Bright field TEM image of a CuO grain reduced to Cu and ED pattern taken from the entire grain. (b) Section of (a).

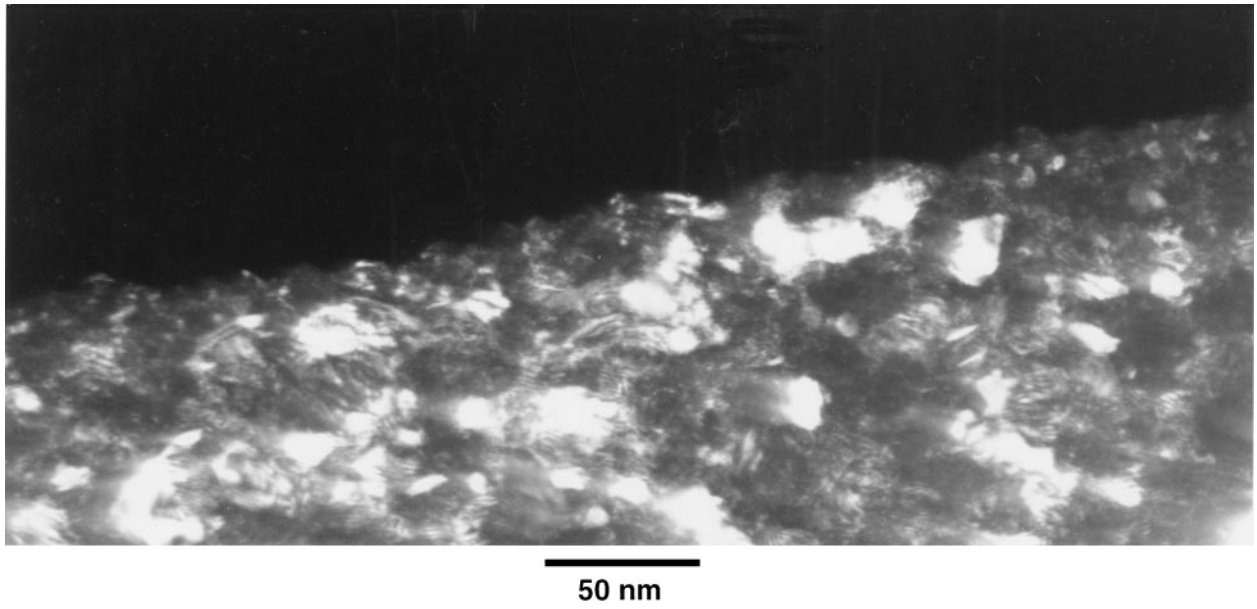

Figure 6 Dark field (from 111) TEM image of an edge of a CuO grain reduced to Cu.

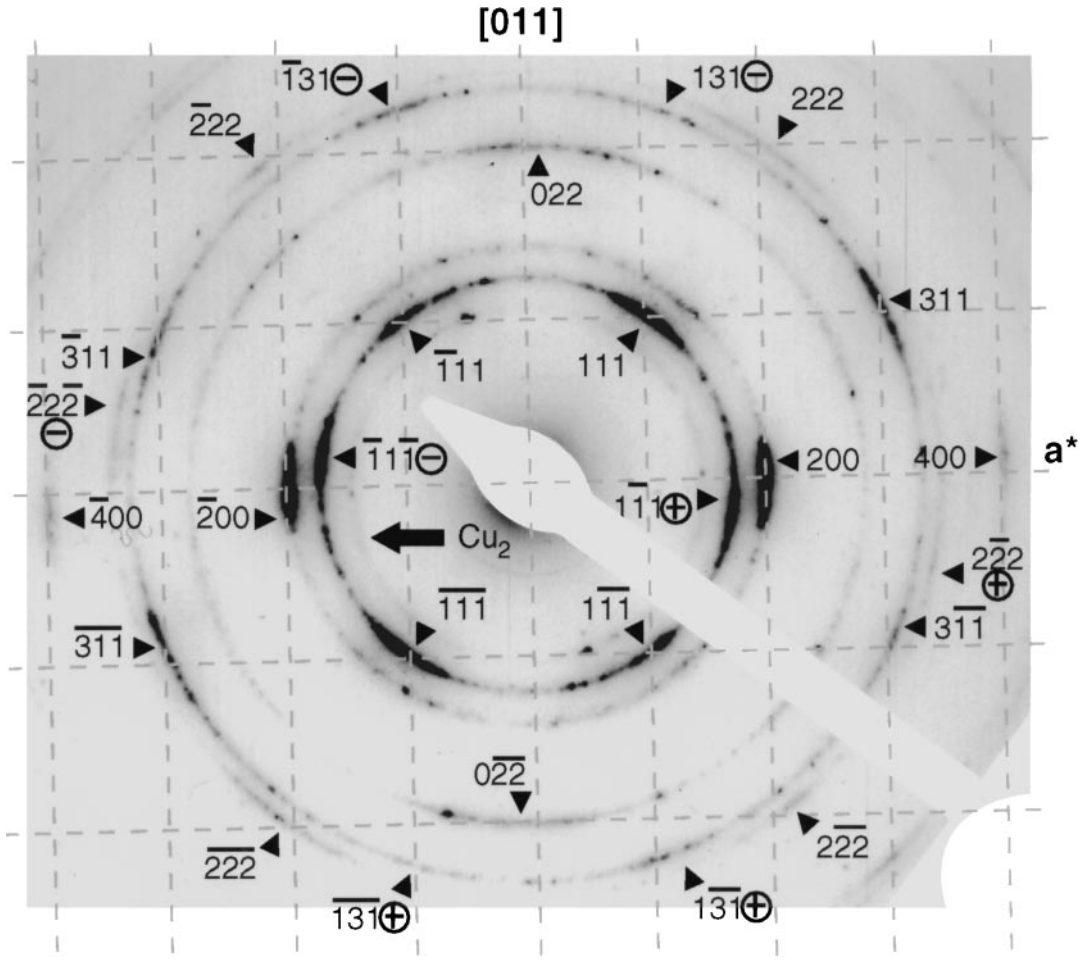

Figure 7 Processed and indexed diffraction pattern from Fig. 5a. The indices correspond to diffuse diffraction spots at or near the [100]/[011] plane of a single crystal, i.e. the [100]/[011] plane of the main direction of strongly textured polycrystalline material. Marks and grid are explained in the text. The weak inner ring labeled as Cu_2 arises from Cu_2O.

of the educt crystals is not possible. To fix the orientational relationship problems partially reduced Cu_2O single crystals were investigated again. As in the SEM study the reaction front was accompanied by a crack which had slightly transparent edges (Fig. 8). ED and dark field imaging proved that one side of the crack is single crystalline Cu_2O, whereas the other side consists of nanocrystalline Cu. ED over the entire area (Fig. 8) provides a direct correlation of the crystal orientations of both parts. The projection shown in Fig. 8 is quite unusual and yields less information (a rotation of the sample led to a blocking of the view of the transparent

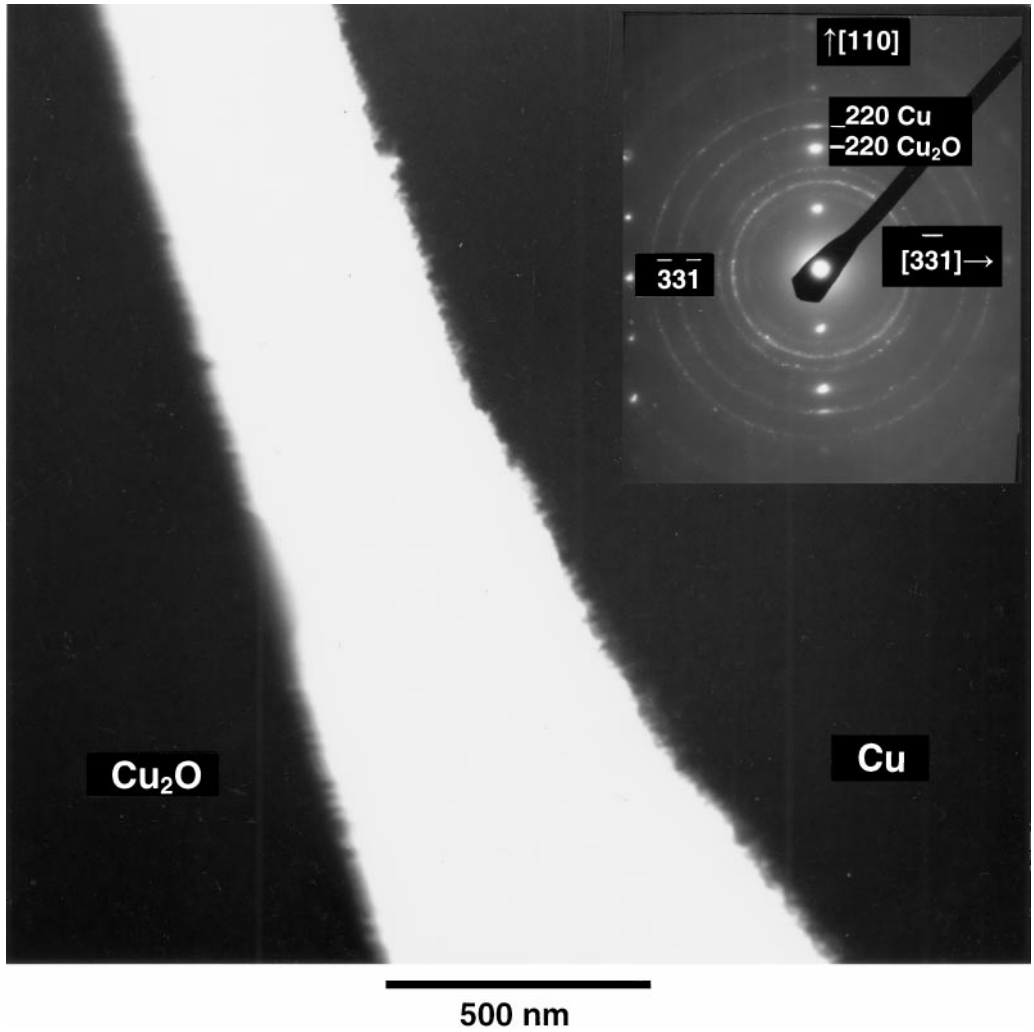

Figure 8 TEM image and ED pattern of a partially reduced Cu_2O single crystal. The Cu_2O and Cu parts are separated by a tear. The ED pattern is a superposition of single crystal spots of Cu_2O ([3$\bar{3}$1]/[110] plane) and inhomogeneous rings of textured nanocrystalline Cu.

region). The Cu 220 reflexes show a spot-like intensity distribution in-line with the 110 single-crystal reflexes of Cu_2O. This provides strong evidence for the coincidence of the {110} net planes of both phases.

3.5. Control of morphology and reactivity

Both size and microstrain were examined using XRD in order to study the dependence of the morphology of the nanocrystals on the preparation conditions. XRD represents a fingerprint method which is better suited than electron microscopy for comparing a series of samples. Preliminary results based on the use of the Scherrer equation yielded an average crystal diameter of 20 and 12 nm for samples prepared at 20 and -40°C, respectively [4].

The diffractograms, in particular the line widths, were found to be independent of the electrochemical method employed, the potential or current density (i.e. reaction kinetics), and the electrolyte (composition and concentration). In addition, the pellets were spatially homogeneous, i.e. the surface particles had the same properties as the bulk ones.

Samples prepared at different temperatures, however, gave significantly different diffractograms resulting in different size and strain parameters (Fig. 9). The

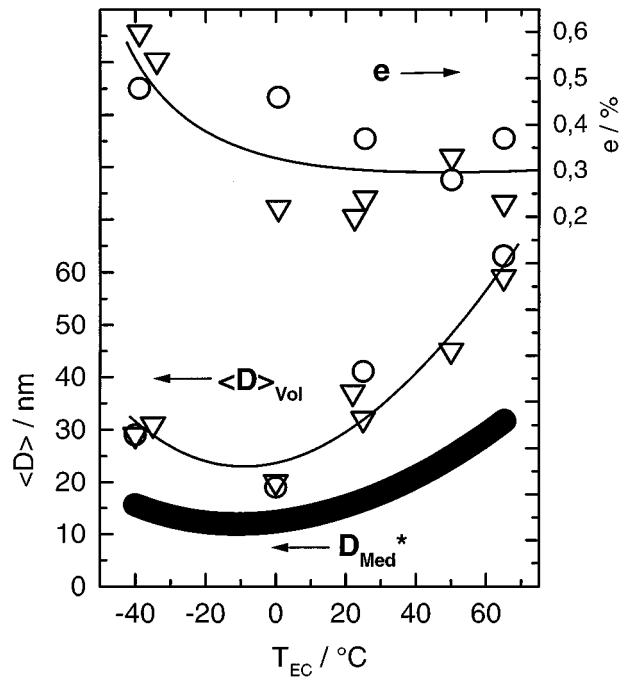

Figure 9 Volume weighted particle size $<D>_{Vol}$ and microstrain parameter e determined by XRD analysis (circles: Warren-Averbach; triangles: Williamson-Hall evaluation) as well as estimated mean particle diameter D^*_{Med} of nanocrystalline Cu as a function of the preparation temperature.

column length distribution as calculated by the Warren-Averbach method was shown to be rather broad. This led to a significant difference between the volume weighted particle size $<D>_{\mathrm{Vol}}$ and the median of the distribution function D_{Med}, i.e. large grains are strongly overestimated. Moreover the calculations indicated that the number of stacking and/or twin faults is very high and results in reduced apparent crystal sizes when compared to values calculated using the simple Scherrer equation [4]. The value for D_{Med} is strongly dependent on the choice of the distribution function. The usual $<D>_{\mathrm{Vol}}$ values are, therefore, given in Fig. 9 together with those obtained using the Williamson-Hall method. It was estimated from the crystallite size distribution ($1.5 < \sigma < 2.0$) that $<D>_{\mathrm{Vol}}$ is about twice as high as the crystal diameter with the highest abundance D^*_{Med}. The latter represents the actual average crystallite size as evaluated by TEM and coincides well with the D_{Med} values. The results shown in Fig. 9 exhibit a well pronounced trend. The particle size D^*_{Med} is in the order of 10–30 nm and seems to have a minimum around a preparation temperature of 0°C.

The averaged (isotropic) microstrain coefficients calculated using both methods exhibit the following trend (Fig. 9): They are almost constant for preparation temperatures above 0°C and increase drastically with decreasing preparation temperature for those lower than 0°C. Note that the strain coefficients from the Williamson-Hall calculation do not only represent the microstrain but also contributions from stacking faults and twin boundaries. Moreover the Warren-Averbach strain coefficient is given for $D = D_{\mathrm{Med}} \leq D^*_{\mathrm{Med}}$, i.e. small particles with relative high microstrain. The values given in Fig. 9 must, therefore, be considered as upper limits for the microstrain coefficient.

It appears that the reactivity of the nanocrystalline material depends on the crystallite size. The oxidation behavior of crushed pellets was investigated upon heating in 1 mbar oxygen (Fig. 10). The onset temperature assigned to surface oxidation (almost no conversion for polycrystalline Cu) is clearly dependent on the crystal size: the smaller the latter the lower is also the former. Moreover, the conversion for the sample prepared at −40°C was rather low compared to the other samples. This was probably due to enhanced spontaneous oxidation (see above, [8]) between the termination of electrochemical reduction and the start of the heat treatment. The spontaneous oxidation at room temperature in air and the first oxidation step in 1 mbar O_2 at about 100°C appear, therefore, to be the same process. The shift in the onset temperature for a given sample is due to the different oxygen partial pressure.

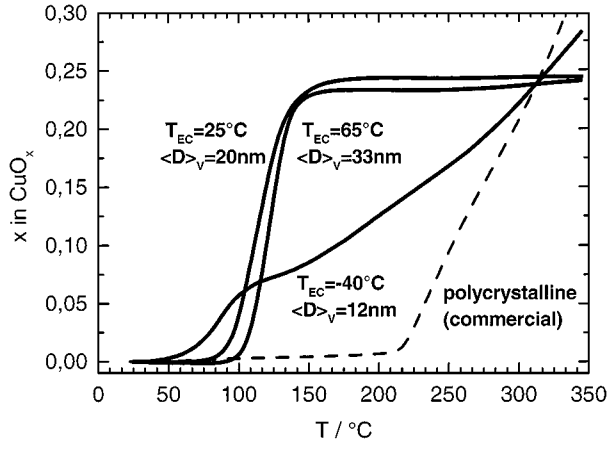

Figure 10 Oxidation behavior (1 mbar O_2, 50 K/h) of copper dependent on the particle size $<D>_{\mathrm{Vol}}$.

4. Discussion

The experimental results described above demonstrate that the electrochemical reduction of copper oxides results in the formation of nanocrystalline and porous copper metal via a solid-solid bulk reaction of the cathode. Since the reaction temperature is markedly below the onset temperatures of strain relaxation or grain growth [9, 10] the observed morphology and measured materials parameters are considered to represent the as-prepared state. That is, unlike as for high temperature reduction methods, crystallite formation and growth (ripening) could be separated.

The reduction of the oxide obviously starts with a fast surface reaction which becomes visible by the color change. The nature of the formed surface species is unknown. One possibility is the formation of highly defective copper oxide (point defects or extended defects) at the sample surface which was found upon decreasing the oxygen partial pressure (first steps of reduction to Cu) at high temperatures [11–13].

It was not the aim of the present study to clarify the mechanism of the bulk reduction, i.e. the structure of Equation 2. Experiments to explore reaction kinetics and deduce rate laws are not discussed here. Nevertheless some remarks are necessary to discuss the morphological properties of the product. The reduction at low temperature is suppressed due to thermodynamic reasons (reaction enthalpy) thus requiring a strong driving force to proceed. Copper oxides are considered commonly to be cation defective and metal (formally: cation vacancy) conductive [11, 14, 15]. The concentration gradient, therefore, would drive a cation motion away from the oxide/metal interface and suppress the reduction. This is a most important difference to the much more intensively studied metal oxidation process. External reactants (as e.g. hydrogen in case of chemical reduction) are not present. Thus the electrochemical potential provides the only possible driving force. Oxygen ions are assumed to be immobile first (but see below). Thus simple decomposition into oxygen and copper ions, i.e. the migration of copper ions to the oxide/metal interface driven by the electrical field is impossible due to charge balance. Charge must be injected as electrons from the metal/oxide interface or as protons from the electrolyte/oxide interface. An injection of electron holes from the electrolyte/oxide interface would lead to hydrogen evolution. This was not observed. Since the electron injection from the metal side cannot solve the problem of oxygen ion oxidation the reduction is expected to proceed as internal decomposition according to Equation 3 for the example Cu_2O.

$$Cu_2O + 2H^+ \rightarrow 2Cu^+ + H_2O \qquad (3)$$

$$2Cu^{+} + 2e^{-} \rightarrow 2Cu \quad (4)$$

The copper ions migrate via vacancies to the oxide/metal interface and are reduced to copper metal (Equation 4). This requires that electronic conductivity in the oxide is negligible. The interfacial contact is maintained by plastical deformation up to a critical degree. The observed texture results from the maximizing of interfacial alignment as it is known for the oxidation [15].

An alternative possibility is based on two significant differences of the reaction described here compared to any chemical high temperature oxidation or reduction: (i) the electrochemical potential provides a most strong driving force for ion motion even at low temperatures; for example topotactical intercalation and deintercalation of oxygen in transition metal oxide ceramics is possible to a much higher extend as by oxidation by molecular oxygen or reduction by molecular hydrogen (e.g. [16]). (ii) electrochemical reactions in aqueous electrolytes provide the participation of protons and thus hydroxyl ions in the reaction both as mobile charge carriers and as reaction partners.

Thus one can assume that under reducing conditions oxygen defects are formed (cf. surface reaction described above) enabling oxygen ion diffusion in copper oxides. Diffusion of hydroxyl anions after injection of protons from the electrolyte (proton assisted oxygen diffusion) is even more probably. The reduction proceeds via topotactic deintercalation of oxygen according to Equation 5 with the formation of water at the electrolyte/oxide interface or, respectively, via the intermediate formation of hydroxyl ions (Equation 6). The anions react with protons to water. This can proceed already at any defects in the bulk due to the diffusion of protons into the oxide. Therefore the diffusion length for oxygen or hydroxyl ions can be short.

$$Cu_2O + 2e^{-} \rightarrow 2Cu + O^{2-} \quad (5)$$

$$Cu_2O + 2e^{-} + H^{+} \rightarrow 2Cu + OH^{-} \quad (6)$$

Since the cations form face centered lattices in Cu, Cu_2O and CuO the topotactical removing of oxygen from any oxide forms copper metal without lattice reconstruction leading directly to the observed structural correlation (and texture) between oxide and metal.

The reaction front should propagate as a sharp oxide/metal interface in the latter model, whereas in the metal-diffusion model the front must be characterized by continuous nonmonotonic changes in the local metal-to-oxygen ratio and a discontinuous ("layer-by-layer") propagation. In each case the reaction is diffusion limited. For comparison, note, that the internal reduction of Cu_2O precipitates in a MgO matrix was observed to result in a Cu/Cu_2O -"patchwork", where Cu and Cu_2O have the same crystallographic orientation [17]. Conversely, reduction of PdO nanocrystals appeared to proceed via the formation of a Pd shell resulting in voids [18]. Since the reaction conditions discussed here differ significantly from these studies (low temperature, large crystals as educt, electrochemical process) one should be careful, however, to compare these results.

The reduction leads formally to a shrinkage (about 40% for both copper oxides) of the solid independent on the local processes. This is due to the difference in the molar volume of oxide and metal. The shrinkage must lead to mechanical stress between the still intergrown (see above) metal and oxide in the oxygen diffusion model. This results in local plastic deformation and finally in fracture. In the metal diffusion model the total volume of the formed metal particles is smaller than the equivalent consumed oxide volume. Since in any case the reduction proceeds locally (at the reaction front) in a practically inelastic matrix of unreacted oxide and already reduced metal, i.e. in a "cavern", the metal cannot be compressed. Consequently unlike as for the metal oxidation the product cannot form a dense structure but must represent a metallic matrix with water inclusions.

Moreover, excess water must be removed via pores since the sum of molar volume of water and metal exceeds that of the oxide. The water can build up a large pressure due to this difference. It is expected that it can burst the grains leading to the separation of the grains and even to cracks within the grains. The same global morphology as in Fig. 1 (macroscopic cracks between grains) was found after hydrogen treatment of oxygen containing copper [19]. This was explained as the consequence of water formation within the copper which bursts the structure. These cracks, however, are expected to become broad only after drying (see below) leading to further shrinking.

The morphological changes seem to proceed in a collective and self-organizing manner resulting in the observed microstructure of crystallite sheets (lamellas). The latter is a consequence of the diffusion control of the reaction. It is obvious that the crystal size of the educt material has no influence on that of the metal product. The latter rather depends on intrinsic properties of the materials participated. This is valid also for the thickness of the lamellas which was found to be homogeneous.

Taking into account the oxygen-diffusion approach, one can assume that in a narrow zone behind the reaction front the oxide is already reduced to copper, but the fragmentation and relaxation is not finished. The apparent density of copper is enhanced, therefore, compared to both the oxide and the nanostructured copper. This may explain the increased EDX signal (Fig. 4e) of Cu behind the oxide/metal interface.

The remaining water bound by capillary forces is removed upon drying and evacuating (note the drop of the O-signal in the EDX line scan in Fig. 4e; the remaining signal is expected to originate from surface reoxidation rather than from oxygen or water inclusions). The matrix further shrinks globally leading to a densification of the nanocrystals within the sheets and the formation of cracks preferred at mechanically weak sites, i.e. grain boundaries (Fig. 1), along lamellas (tears in Figs 1 and 2), oxide/metal interface and defects introduced during excess water removal. This explains the cracks observed at or near the metal/oxide interface by electron microscopy (Figs 4 and 8) which cannot be formed in the course of the reduction. Moreover, the cracks were

not present before reaction thus serving as traps for the reaction front.

The pellets or crystals show no measurable volume change whereas the shrinking of the macroscopic grains after drying is 15–30% (depending on the current density and after drying, see above). Although sintered pellets have a considerable part of macroscopic pores (Fig. 1) these pores are not needed to take into account because they do not participate in the reaction. The nanocrystallites occupy about 70–85% of the grain volume (after drying). Since the space between the lamellas is not considered yet the nanocrystals must be arranged very densely *after drying* (note that closed packed spheres occupy 74% of the total space). It is reasonable from the foregoing arguments to assume a less dense packing after reduction *without drying*.

A variable to control the packing density, i.e. the crystallite/pore volume ratio, is the starting compound, in particular the expected volume change in the course of the reaction. For example, the reduction of CuI (79% volume reduction !) gave a Cu product much more reactive against oxidation than Cu reduced from CuO [4]. This was assigned both to a reduced particle size and to a better accessibility of the particles due to an enhanced porosity.

If the origin of nanocrystal generation is assigned only to the lattice mismatch between oxide and metal resulting in stress and fracture (oxygen diffusion model) the size of the nanocrystals should depend also on the *mechanical* properties of metal and/or oxide. The crystal separation (stress relaxation by fracture) at rather high temperatures ($T > 0^\circ$C) proceeds, when a defined strain ($e = 0.3\%$ according to Fig. 9) is accumulated at the interface. The elasticity of the metal increases with increasing temperature. Therefore the crystal size which is necessary to reach the critical strain also increases. At low temperatures ($<0^\circ$C) the separation of the particles seems to be hindered. More strain is accumulated with decreasing temperature before a nanocrystal tears away, and the particles become larger again.

As mentioned above not all factors which could influence both the process and the product were investigated here. The crystal generation may be determined also by the *diffusion* properties, i.e. by kinetics. Although the latter are model-dependent (see above), in general the crystal size should be dependent on the relevant diffusion coefficient and thus represent an intrinsic (temperature dependent) material parameter. Another critical parameter is the *defect structure* of the oxide. We have to assume that it can influence both the reaction process as well as the morphological properties of the product including the texture.

5. Conclusions

In summary the production of nanocrystalline copper with particle size and microstrain dependent on the preparation temperature as well as a pore structure (density) dependent on the educt and post-treatment (i.e. water content) was demonstrated to be appropriate using simple electrochemical reduction of oxides or salts. Thus the relevant materials parameters, i.e. crystallite size and relative pore volume, can be controlled separately. They were found to be spatially homogeneous and dependent rather on the materials properties than on the process parameters. Crystallite formation could be separated from grain growth/ripening due to the low processing temperature thus conserving the as-prepared crystallite size. Consequently it appears possible to use this approach as a most easy production strategy for nanocrystalline porous metals (Cu, Ag, Bi) without critical process parameters.

Acknowledgements

We thank R. Schöllhorn for fruitful discussion and support. This work was partially supported by the Deutsche Forschungsgemeinschaft.

References

1. H. HAHN, *Nanostructured Mater.* **9** (1997) 3.
2. C. C. KOCH, *ibid.* **9** (1997) 13.
3. H. NATTER, T. KRAJEWSKI and R. HEMPELMANN, *Ber. Bunsenges. Phys. Chem.* **100** (1996) 55.
4. G. PFLETSCHINGER, B. HAHN and R. SCHÖLLHORN, *Solid State Ionics* **84** (1996) 151.
5. O. PYPER, B. HAHN and R. SCHÖLLHORN, *J. Mater. Chem.* **7** (1997) 465.
6. H. NATTER, Dissertation, Saarbrücken, 1996.
7. G. K. WILLIAMSON and W. H. HALL, *Acta Metallurgica* **1** (1964) 22.
8. J. URBAN, H. SACK-KONGEHL and K. WEISS, *Z. Phys. D* **36** (1996) 73.
9. S. R. AGNEW and J. R. WEERTMAN, *Mat. Sci. Eng.* **A242** (1998) 174.
10. V. Y. GERTSMAN, R. BIRRINGER, R. Z. VALIEV and H. GLEITER, *Sripta Metall. Mater.* **30** (1994) 229.
11. O. PORAT and I. RIESS, *Solid State Ionics* **74** (1994) 229.
12. *Idem., ibid.* **81** (1995) 29.
13. V. A. SADYKOV, S. F. TIKHOV, G. N. KRYUKOWA, N. N. BULGAKOV, V. V. POPOVSKII and V. N. KOLOMIICHUK, *J. Solid State Chem.* **73** (1988) 200.
14. C. WAGNER, *Progr. Solid State Chem.* **10** (1975) 3.
15. W. W. SMELTZER and D. J. YOUNG, *ibid.* **10** (1975) 17.
16. A. NEMUDRY, M. WEISS, I. GAINUTDINOV, V. BOLDYREV and R. SCHÖLLHORN, *Chem. Mater.* **10** (1998) 2403.
17. M. BACKHAUS-RICOULT and S. HAGÈGE, *Phil. Mag. A* **67** (1993) 1471.
18. P. A. CROZIER, R. SHARMA and A. K. DATYE, *Microsc. Microanal.* **4** (1998) 278.
19. H. SCHUMANN (ed.), "Metallographie," 13th ed. (Deutscher Verlag für Grundstoffindustrie, Leipzig) p. 629.
20. B. E. WARREN, in "Progress in Metal Physics," edited by B. Chalmers and R. King (Pergamon Press, New York, 1959) p. 147.

Received 7 October 1999
and accepted 18 February 2000